Available online at www.sciencedirect.com
SCIENCE DIRECT
Thermochimica Acta 414 (2004) 53–58
thermochimica acta
www.elsevier.com/locate/tca

Spectroscopic and thermal properties of $FeHg(SCN)_4$

X.Q. Wang [a,*], D. Xu [a], M.J. Liu [b], X.Q. Hou [a,c], X.F. Cheng [a], M.K. Lu [a], D.R. Yuan [a], J. Huang [d]

[a] State Key Laboratory of Crystal Materials, Institute of Crystal Materials, Shandong University, Jinan 250100, PR China
[b] Qingdao Institute of Architecture and Engineering, Qingdao 266033, PR China
[c] School of Materials Science, Jinan University, Jinan 250022, PR China
[d] College of Environmental Science and Engineering, Institute of Modern Analysis, Shandong University, Jinan 250100, PR China

Received 5 May 2003; received in revised form 7 November 2003; accepted 7 November 2003

Abstract

The preparation and characterization of iron mercury thiocyanate, $FeHg(SCN)_4$ (abbreviated as FMTC) are described. The spectroscopic properties were characterized by X-ray powder diffraction (XRPD), infrared, Raman and UV-Vis-NIR transmission spectra. The thermal stability and thermal decomposition of FMTC were investigated by means of thermogravimetric analysis (TGA) and differential thermal analysis (DTA). The intermediates and final products of the thermal decomposition were identified by X-ray powder diffraction at room temperature.

Keywords: Iron mercury thiocyanate; X-ray powder diffraction; Infrared spectroscopy; Raman spectroscopy; Transmission spectra; Thermal analysis

1. Introduction

Recently, good second-order nonlinear optical (SONLO) materials capable of efficient frequency conversion of infrared laser radiation to visible and ultraviolet wavelengths are attracting much attention since they are of great interest for applications including telecommunications, optical computing, optical information processing, optical disk data storage, laser remote sensing, laser-driven fusion, color displays, medical diagnostics, etc. Materials with large second-order optical nonlinearities, short transparency cutoff wavelengths and stable physicochemical performances are needed in order to realize many of these applications.

The $MHg(SCN)_4{\cdot}nH_2O$ (where M = Co, Cu, Zn, Cd, Ni, Fe, Mn) series of crystalline complexes have been known for a century in analytical chemistry for their characteristic shapes and colors [1]. Along with the development of nonlinear optics, such coordination compounds have been discovered to be useful as SONLO materials [2,3]. In recent years, the more detailed preparation, structure and SONLO properties of $MHg(SCN)_4$ (M = Cd, Zn, Mn, abbreviated as CMTC, ZMTC and MMTC, respectively) crystals were reported [4–7]. The crystal structure and SONLO properties of iron mercury thiocyanate ($FeHg(SCN)_4$, abbreviated as FMTC hereafter) crystal were reported previously [8]. It belongs to the tetragonal crystallographic system, space group $I\bar{4}$, with cell parameters $a = 11.1244(2)$ Å, $c = 4.2890(10)$ Å, $V = 542.2(2)$ Å^3, $Z = 2$, $D_c = 2.993$ g/cc. FMTC crystal powder shows a 532 nm second harmonic intensity 0.6 times as that of the urea crystal powder. To continue this work, in this paper, the spectroscopic properties of FMTC are investigated by X-ray powder diffraction (XRPD), infrared (IR), Raman and UV-Vis-NIR transmission spectra. The thermal properties of the complex are studied by thermogravimetric analysis and differential thermal analysis (TGA/DTA) in combination with XRPD phase analysis of the solid residues at room temperature.

2. Experimental

2.1. Materials and synthesis

All the starting materials were analytical reagent grade (purity ≥ 98.0%) and used as purchased. FMTC was syn-

* Corresponding author. Tel.: +86-531-8362822; fax: +86-531-8565403.
E-mail address: xqwang@icm.sdu.edu.cn (X.Q. Wang).

0040-6031/$ – see front matter
doi:10.1016/j.tca.2003.11.010

thesized by a coordination reaction and then a metathetical reaction, where M = K, Na, NH_4:

$$4MSCN + HgCl_2 = M_2Hg(SCN)_4 + 2MCl$$

$$M_2Hg(SCN)_4 + FeCl_2 = FeHg(SCN)_4 + 2MCl$$

2.2. Physical measurements

The XRPD pattern of FMTC product was registered with a Rigaku D/Max-γA diffractometer, operated at 40 kV and 40 mA, using a Cu target (λ = 1.54178 Å) tube and a graphite monochrometer. Fixed scatter and divergence slits of 1° and a 0.15 mm receiving slit were used. The intensity data were recorded by continuous scan in a 2θ–θ mode from 10 to 70° with a step size of 0.02° and a scan speed of 4°/min.

The IR spectrometry measurement of FMTC product was carried out by use of a Nicolet 750 FTIR spectrometer at room temperature in the 4000–400 cm^{-1} region. The Raman spectrum of FMTC product was measured on a LABRAM microscopic Raman spectrometer with a slit width of 100 nm, using a 100 mW Argon ion laser at 514.53 nm with a power density of 5 $mW/\mu m^2$ at the sample.

FMTC and CMTC (0.04 mmol each) were dissolved in 100 ml of a mixed solvent of ethanol and water (1:1=V:V), respectively. Using the above-mentioned solvent as reference, the transmission spectra in the wavelength range 200–1000 nm of the two solutions were obtained on a Hitachi model U-3500 spectrometer using a matched pair of 1 cm quartz cuvettes.

TGA/DTA were carried out in the temperature range of 50–1500 °C by using of a Netzsch simultaneous thermal analyzer (model STA409) under air flux, at a heating rate of 10 °C/min. In order to examine the course of thermal decomposition of the compounds under study, the solid samples were heated and decomposed to various temperatures: 200, 330, 370, 500, 600 and 900 °C in the furnace within an open Pt crucible under air atmosphere. The cooled residues were removed from the crucible and subjected to XRPD analysis as stated above.

3. Results and discussion

3.1. X-ray powder diffraction

The original XRPD pattern of FMTC was reported previously (JCPDS No. 20-523). However, it was not completed. The tetragonal unit-cell parameters calculated by DICVOL91 [9,10] program, according to the values of 2θ in XRPD pattern are $a = 11.2407$ Å, $c = 4.2909$ Å, $V = 542.17$ $Å^3$, which are more consistent with the results determined by an R3m/E four-circle X-ray diffractometer [8] than the original data. The XRPD data for FMTC are tabulated in Table 1.

Table 1
Relative experimental intensities, *d*-spacings (observed and calculated), 2θ (observed and calculated) and their indices for FMTC product

h	*k*	*l*	d_{obs} (Å)	d_{calc} (Å)	$2\theta_{obs}$ (°)	$2\theta_{calc}$ (°)	I/I_0 (%)
1	1	0	7.951	7.9484	11.128	11.131	77
2	0	0	5.622	5.62037	15.762	15.767	63
1	0	1	4.007	4.00873	22.182	22.174	63
2	2	0	3.975	3.9742	22.363	22.37	100
3	1	0	3.556	3.55463	25.043	25.05	20
2	1	1	3.263	3.26364	27.329	27.325	63
3	0	1	2.822	2.82231	31.703	31.703	49
3	3	0	2.647	2.64947	33.862	33.831	51
4	2	0	7.951	2.5135	35.671	35.721	83
4	1	1	2.301	2.30109	39.156	39.146	30
4	3	0	2.249	2.24815	40.093	40.107	6
5	0	0					
1	1	2	2.071	2.07131	43.717	43.7	5
4	4	0	1.988	1.9871	45.634	45.654	53
5	3	0	1.928	1.92777	47.148	47.142	18
5	2	1	1.876	1.87704	48.531	48.497	27
3	1	2	1.837	1.8368	49.614	49.63	19
6	2	0	1.777	1.77732	51.407	51.41	19
6	1	1	1.698	1.69725	54.008	54.027	13
3	3	2	1.667	1.66733	55.086	55.078	4
5	4	1	1.625	1.62478	56.641	56.648	9
5	5	0	1.589	1.58968	58.029	58.016	12
7	1	0					
6	4	0	1.559	1.55881	59.281	59.279	20
5	1	2	1.538	1.5375	60.159	60.184	12
7	0	1	1.504	1.50395	61.657	61.671	2
7	2	1	1.453	1.45283	64.073	64.093	8
5	3	2	1.434	1.43394	65.044	65.041	4
8	0	0	1.405	1.40509	66.544	66.548	5
6	5	1	1.364	1.36452	68.825	68.798	12

3.2. IR and Raman spectra

The main IR spectral data of FMTC and KSCN [11] are listed in Table 2. It can be seen that the wavenumbers of the CN and CS stretching vibration peaks in FMTC are much higher than that in free SCN radical of KSCN. Meanwhile, the wavenumbers of SCN bending vibration peaks of FMTC show a clear contrary in tread. This can be explained by the electron transformation model [12,13]. In FMTC, N and S in SCN^- are good electron-donors, and at the same time, Fe^{2+} and Hg^{2+} are both strong electron-acceptors. The coordination of N and S to Fe^{2+} and Hg^{2+}, respectively make the wavenumbers of CN and CS stretching vibration increase significantly and those of SCN bending vibration decrease.

The Raman spectrum of FMTC consists of four frequency regions (below 100 cm^{-1}, lattice vibration modes;

Table 2
Comparison of the main IR spectral data (cm^{-1}) of FMTC with KSCN

Assignment	FMTC	KSCN
ν(CN)	2082.37, 2116.20, 2130.80	2063
ν(CS)	784.69	746
δ(NCS)	427.11, 444.49, 467.98	488
2δ(NCS)	891.47, 934.75	940

Table 3
Observed Raman vibrational spectra data (cm^{-1}) and their assignments of FMTC product in the 50–2500 cm^{-1} range

Raman spectra	Assignments
61.36, 73.74	Lattice mode
105.48	δ(Hg–SCN–Fe)
123.07	δ(S–Hg–S)
233.08	δ(N–Fe–N)
447.35, 467.64, 479.46	δ(SCN)
782.64	ν(CS)
881.29, 913.37, 929.37, 973.38	2δ(SCN)
2078.76, 2114.82, 2142.45	ν(CN)

100–300 cm^{-1}, vibration bands of Hg and Fe centers; 300−1200 cm^{-1}, SCN internal vibration modes; 2100−2200 cm^{-1}, CN stretching vibration modes). All the Raman lines at the low wavenumber are very broad, and the intensity and count background of all scattering configurations at the low wavenumber are very strong. According to the vibrational spectra [14–17], the observed Raman bands along with their vibrational assignments are summarized in Table 3. The Raman peaks are not split but broaden on the low-wavenumber side owing to the distortion of the $Fe(NCS)_4$ and $Hg(SCN)_4$ tetrahedra in FMTC crystal.

3.3. Optical transmission study

Since single crystals are mainly used in optical applications, the optical transmission range and the transparency cutoff are important. Because FMTC easily decomposes in its molten state and it is not sublimable, the entire crystallization process is performed in solution. However, the growth of FMTC is very difficult due to the instability of its growth solutions which are easily oxidated in air. Till now, no considerably large crystal suitable for determining its transmission spectrum has been obtained. The transmission spectrum can be studied by recording the transmission spectra of its solution.

The transmission spectra of FMTC and CMTC solutions are shown in Fig. 1, which shows that the transparency cutoffs of FMTC and CMTC in such solution states occur at 303 and 291 nm, respectively. From which, one can see that the UV transparency cutoff of FMTC is shifted to red band compared with that of CMTC, which must be due to the low-energy d–d transmissions of Fe^{2+} whose electronic configuration is $3d^6$.

3.4. Thermal properties

The simultaneously recorded TGA/DTA curves of FMTC are shown in Fig. 2. FMTC starts its decomposition at 219.4 °C. The TGA curve shows the process of thermal dissociation: breakdown of the three-dimensional steric structure (3DSS) and the formation of the corresponding metal(II)-sulfides, carbon dioxide (CO_2), nitrogen gas (N_2), sulfur dioxide (SO_2) and ferric oxide (Fe_2O_3). Most of the volatile degradation products were released until 400 °C, but the weight losses were continued further with rising temperature. $FeHgS_2$ was formed already at relatively low temperatures, but not exclusively. The behavior of evolved sulfides was the continuous sublimation and loss of HgS and the formation of $FeHg_{(1-x)}S_{(2-x)}$. There was a plateau in the range of 450–600 °C.

DTA curve presents three steps. The first one between 50 and 400 °C, which is the breakdown of the 3DSS and the formation small-molecule compounds; the second and the

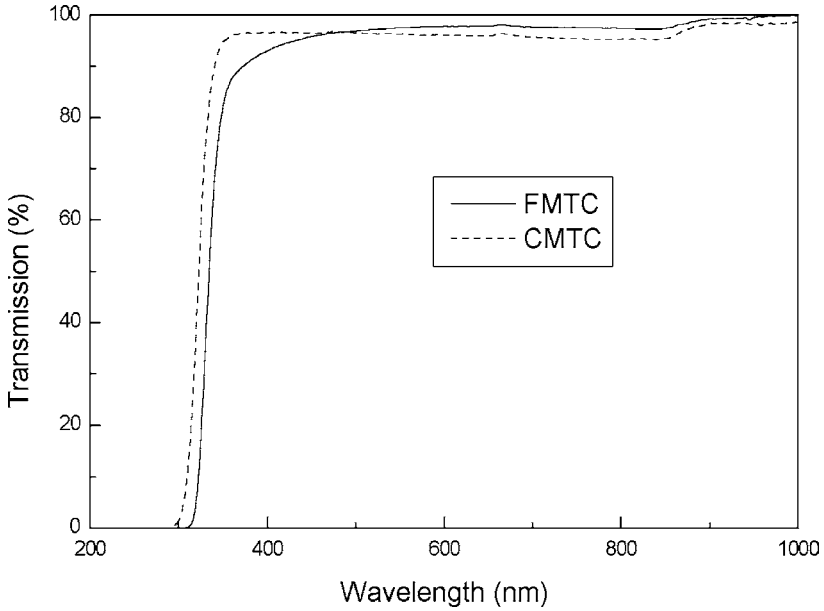

Fig. 1. Transmission spectra of FMTC and CMTC in their 0.4 mM solutions.

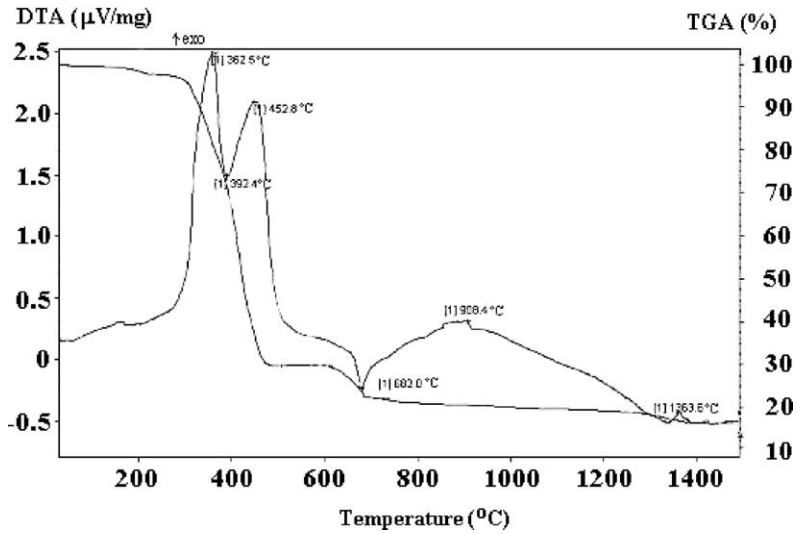

Fig. 2. TGA/DTA curves of FMTC.

third one, which extends up to 700 and 1400 °C, respectively. The analysis of the three principal steps shows that the first implies a loss of 4C($4CO_2$), 4N($2N_2$) and 2S(SO_2), and the solid remainder is $FeHgS_2$. Second exhibits a continuous loss of HgS and the formation of $FeHg_{(1-x)}S_{(2-x)}$, but no occurrence of FeS was detected till its oxidation. Third is the oxidation and the formation of the weight constant final oxide (Fe_2O_3). DTA presents four exothermic and two endothermic peaks located respectively at 362.5, 392.4, 452.8, 682.0, 908.4 and 1363.6 °C accompany with the degradation. The first two is related to the first TGA step, i.e. the breakdown of 3DSS and the elimination of the volatile gases. The second two is related to the second step, i.e. the sublimation of HgS and the formation of part Fe_2O_3. The third two is related to the third step, i.e. the formation of Fe_2O_3. The XRPD patterns of the sinter for each temperature: 200, 330, 370, 500, 600 and 900 °C are exhibited in Fig. 3(a)–(f), respectively. Fig. 3(a) exhibits that the product is still the tetragonal phase FMTC. Fig. 3(b) and (c) shows that the product obtained are cubic phases. Judged by other mixed sulfides in the old literatures (JCPDS Nos. 2-0463, 5-0566, 6-0261, 22-731, 50-1151), one can presume they must be new phases: $FeHgS_2$ and $FeHg_{(1-x)}S_{(2-x)}$ ($0 < x < 1$). The structure of $FeHgS_2$ were derived from powder X-ray diffraction data, and the cubic unit-cell parameters calculated by DICVOL91 program according to the values of 2θ in the XRPD patterns are $a = 5.8402$ Å, $V = 199.19$ Å^3. The XRPD data for $FeHgS_2$ are listed in Table 4. There is an increasing demand on low-cost compound-semiconductor thin films consisting of single and complex metal sulfides obtained by spray pyrolysis deposition (SPD) [18]. Therefore, metallic thiocyanates, for example FMTC, can be used as the sources to obtained metal sulfides by SPD. Fig. 3(d)–(f) shows that the main residue is Fe_2O_3 (JCPDS No. 33-664). In fact, the mechanism concerning of the thermal decomposition of FMTC would be the formation of both mixed iron mercury sulfides and Fe_2O_3 as by product. Fe_2O_3 was not observed by XRPD must be due to the very small particle sizes of Fe_2O_3 at relatively low temperatures. However, with the increase of the temperature, these tiny particles would grow into large size and be observed. The thermoanalytical data of FMTC are exhibited in Table 5.

Table 4
Relative experimental intensities, *d*-spacings (observed and calculated), 2θ (observed and calculated) and their indices for $FeHgS_2$

h	*k*	*l*	d_{obs} (Å)	d_{calc} (Å)	$2\theta_{obs}$ (°)	$2\theta_{calc}$ (°)	I/I_0 (%)
1	1	1	3.371	3.37181	26.425	26.433	100
2	0	0	2.915	2.92008	30.636	30.615	38
2	2	0	2.063	2.06481	43.836	43.844	50
3	1	1	1.762	1.76087	51.828	51.926	42
2	2	2	1.682	1.68591	54.512	54.42	15

Table 5
Thermoanalytical data of FMTC

TGA temperature (°C)	Stage	DTA peak temperature (°C)	Weight loss (%)		Evolved moiety
			Observed	Calculated	
50–400	1	362.5, 392.4	32.5	34.4	CO_2, N_2, SO_2, $FeHgS_2$
400–700	2	452.8, 682.0,	48.8	47.6	$FeHg_{(1-x)}S_{(2-x)}$ ($0 < x < 1$), HgS, FeS, Fe_2O_3
700–1400	3	908.4, 1363.6	2.1	1.6	Fe_2O_3
>1400	Residue				Fe_2O_3

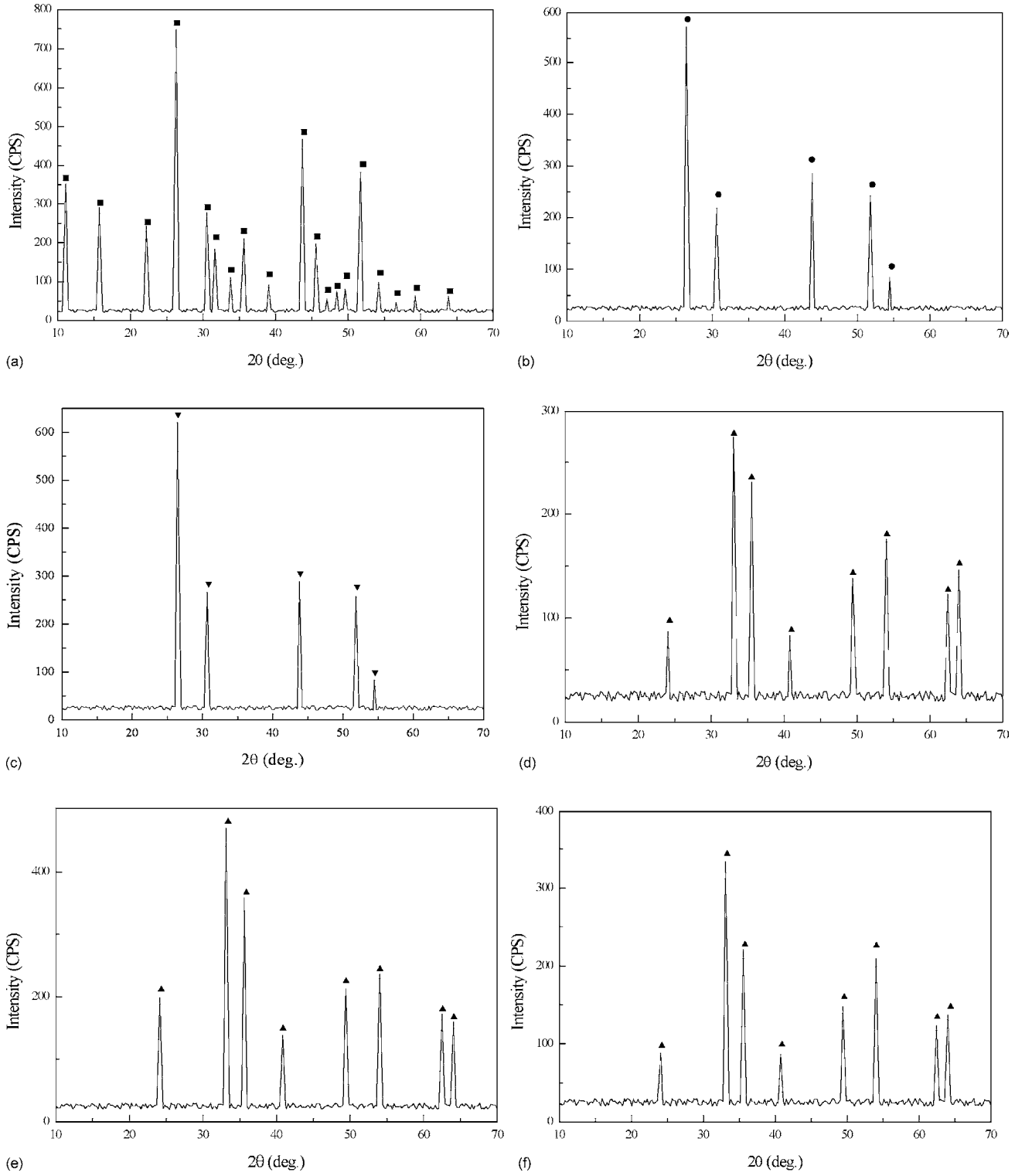

Fig. 3. XRPD patterns at room temperature of the sinters of FMTC at 200 °C (a), 330 °C (b), 370 °C (c), 500 °C (d), 600 °C (e) and 900 °C (f): (■) $FeHg(SCN)_4$; (●) $FeHgS_2$; (▼) $FeHg_{1-x}S_{2-x}$ ($0 < x < 1$); (▲) Fe_2O_3.

According to above-mentioned analyses, we presume that the following reaction scheme is the most reasonable to describe the decomposition process (where $0 \leq x \leq 1$):

$$FeHg(SCN)_4 + 4O_2 \rightarrow FeHg_{(1-x)}S_{(2-x)} + 2CO_2 + 2SO_2 + 2N_2 + x\,HgS$$

$$FeHg_{(1-x)}S_{(2-x)} + O_2 \rightarrow Fe_2O_3 + (1-x)HgS + SO_2$$

4. Conclusions

The preparation of FMTC has been described. Spectroscopic properties have been established by using various ways. The structure of FMTC were derived from powder X-ray diffraction data, and the tetragonal unit-cell parameters calculated by DICVOL91 program according to the values of 2θ in the XRPD patterns are $a = 11.2407$ Å, $c = 4.2909$ Å, $V = 542.17$ Å^3, which are comparable with the results determined by an R3m/E four-circle X-ray diffractometer. Its vibrational spectra were studied by IR and Raman spectroscopy, which show that the characteristic vibrational modes of $FeHg(SCN)_4$ crystals consist of six wavenumber regions: below 100 cm^{-1}, lattice vibration modes; 100–300 cm^{-1}, vibration bands of Hg and Fe centers ($Hg(SCN)_4$ and $Fe(NCS)_4$ bending vibration modes); 300–500 cm^{-1}, an SCN bending vibration mode; 750–800 cm^{-1}, a CS stretching vibration mode; 850–950 cm^{-1}, a doubly degenerate SCN bending vibration mode; 2100–2200 cm^{-1}, a CN stretching vibration mode. The optical transmission spectrum exhibits that the UV transparency of FMTC is inferior to that of CMTC. The TGA/DTA analyses reveal that the thermal decomposition of FMTC in air is breakdown of the 3DSS and the formation of the corresponding metal(II)-sulfides ($FeHg_{(1-x)}S_{(2-x)}$ ($0 \leq x \leq 1$)), carbon dioxide (CO_2), nitrogen gas (N_2), sulfur dioxide (SO_2) and ferric oxide (Fe_2O_3). From the thermal decomposition scheme, one can see that metallic thiocyanates can be used as the sources to obtain the low-cost compound–semiconductor thin films consisting of metal sulfides.

Acknowledgements

This work is supported by an "863" grant (No. 2002AA313070) National Advanced Materials Committee of China (NAMCC), a grant (No. 50272037) of National Natural Science Foundation of China (NNSFC), the Youth Science Foundation of Shandong University (No. 11370053187029) and the Doctoral Startup Foundation of Shandong University (No. 10000052182149).

References

[1] A. Rosenheim, R. Cohn, Z. Anorg. Allgem. Chem. 27 (1901) 280.
[2] J.G. Bergman, J.J. Mcfee, G.R. Crane, Mater. Res. Bull. 5 (1970) 913.
[3] W. Sturmer, U. Deserno, Phys. Lett. A 32 (1970) 539.
[4] D.R. Yuan, M.G. Liu, D. Xu, Q. Fang, W.T. Yu, W.B. Hou, Y.H. Bing, S.Y. Sun, M.H. Jiang, Appl. Phys. Lett. 70 (1997) 544.
[5] D. Xu, W.T. Yu, X.Q. Wang, D.R. Yuan, M.K. Lu, P. Yang, S.Y. Guo, F.Q. Meng, M.H. Jiang, Acta Cryst. C 55 (1999) 1203.
[6] Y.X. Yan, Q. Fang, D.R. Yuan, Y.P. Tian, Z. Liu, X.M. Wang, M.H. Jiang, D. Williams, A. Siu, Z.G. Cai, Chin. Chem. Lett. 10 (1999) 257.
[7] X.Q. Wang, D. Xu, M.K. Lu, D.R. Yuan, G.H. Zhang, F.Q. Meng, S.Y. Guo, M. Zhou, J.R. Liu, X.R. Li, Cryst. Res. Technol. 36 (2001) 73.
[8] Y.X. Yan, Q. Fang, W.T. Yu, Y.P. Tian, D.R. Yuan, X.Q. Wang, F.Q. Meng, Z.G. Cai, L.Z. Zhang, Chin. Chem. Lett. 9 (1998) 1125.
[9] D. Louer, M. Louer, J. Appl. Cryst. 5 (1972) 271.
[10] A. Boultif, D. Louer, J. Appl. Cryst. 24 (1991) 987.
[11] P.O. Kinell, B. Strandberc, Acta Chem. Scand. 13 (1959) 1607.
[12] C. Balarew, R.J. Duhlew, Solid State Chem. 55 (1984) 1.
[13] K. Nakamoto, translated by D.R. Huang, R.Q. Wang, Infrared and Raman Spectra of Inorganic and Coordination Compounds, 4th ed., Chemical Industry Press, Beijing, 1991, p. 304 (in Chinese).
[14] J. Lewis, R.S. Nyholm, P.W. Smith, J. Chem. Soc. 83 (1960) 1992.
[15] A. Sabatini, I. Bertini, Inorg. Chem. 4 (1965) 959.
[16] A. Muller, K.H. Schmidt, K.H. Tytko, J. Bouwma, F. Jellinek, Spectrochim. Acta 28A (1972) 381.
[17] G.J. Kubas, L.H. Jones, Inorg. Chem. 13 (1974) 2816.
[18] J. Madarasz, P. Bornbicz, M. Okuya, S. Kaneko, Solid State Ionics 141–142 (2001) 439.